KSME

Springer

Journal of Mechanical Science and Technology 35 (12) 2021

Original Article
DOI 10.1007/s12206-021-1144-5

Keywords:
· Entropy generation
· Hybrid heat sink
· Jet impingement
· Microchannel heat sink
· Thermal resistance

Correspondence to:
Mohd. Zahid Ansari
zahid@iiitdmj.ac.in;
Afzal Husain
afzal19@squ.edu.om

Citation:
Pandey, J., Zahid Ansari, M., Husain, A. (2021). Performance analysis of hybrid microchannel heat sink for varying nozzle geometry and layout on the basis of first- and second-law of thermodynamics. Journal of Mechanical Science and Technology 35 (12) (2021) 5753~5764. http://doi.org/10.1007/s12206-021-1144-5

Received April 12th, 2021
Revised July 17th, 2021
Accepted August 29th, 2021

† Recommended by Editor Tong Seop Kim

Performance analysis of hybrid microchannel heat sink for varying nozzle geometry and layout on the basis of first- and second-law of thermodynamics

Jyoti Pandey[1], Mohd. Zahid Ansari[1] and Afzal Husain[2]

[1]MEMS & Microfluidics Lab, Mechanical Engineering Discipline, PDPM-Indian Institute of Information Technology Design and Manufacturing, Airport Road, Jabalpur 482005, MP, India, [2]Department of Mechanical and Industrial Engineering, Sultan Qaboos University, Muscat, Oman

Abstract This paper investigates the enhanced cooling performance of a hybrid microchannel heat sink, consists of the microchannel, nozzle and pillars, in terms of various hydrothermal characteristic parameters. Geometric and flow variables such as jet inclination angle (30°-90°), Reynolds number (200-600) and nozzle diameter (in increasing/decreasing order) are considered for the analysis. Parameters related to both the first and second laws of thermodynamics are computed numerically using commercial software ANSYS FLUENT. The decreasing nozzle diameter layout provided the lowest value of the maximum wall temperature as well as a moderate hike in the pressure drop with respect to other cases. Similarly, a smaller nozzle angle is more suitable for better cooling than the larger nozzle angles.

1. Introduction

The electronic cooling problem is becoming more complex with time due to non-linearly escalating power density every year. Unrestrained heat dissipation in electronic circuits extended the heat flux value beyond 1000 W/cm^2 due to the integration of large-scale tiny components over micro-scaled chips. Electronic devices thermal characteristics reached critical value owing to a huge amount of heat flux generation in the micro-sized appliances. Reported studies revealed several conventional techniques developed and tested to design consistent and adequate cooling system. These traditional methods such as finned cold plate/heat sink, microchannel heat sink, etc., are predominantly based on conduction and air-induced free or forced convection heat transfer modes. The liquid-cooled microchannel heat sink was a remarkable discovery in the cooling applications proposed by Tuckerman and Pease [1] in 1981 using water as coolant for VLSI circuit having heat flux density up to 790 W/cm^2. But, these heat mitigation solutions become inadequate for the current high cooling requirement due to the small surface area available and laminar flow in the microchannel. Thus, the thermal management system needs evolution where new techniques must be capable of reducing thermal resistance by diminishing thermal boundary layer, enhancing fluid mixing, or causing turbulence locally in the flow. Later on, several modifications in channel geometry [2, 3] and in designs were incorporated with various active and passive techniques to enhance conduction and convection heat transfer or to minimise thermal resistance, pressure drop and boundary layer thickness [4-11]. Among these methods, the jet impingement cooling technique found highly effective in maintaining device temperature below the threshold limit because of the ability to disturb and penetrate the thick laminar flow bed.

Jet impingement is a process to achieve a high amount of heat transfer in a short time by projecting the fluid vertically over the surface at high velocity [12]. A high local heat transfer

coefficient obtained on the target surface commonly elevates the convective heat transfer rate. This is attributed to a reduction of hydrodynamic and thermal boundary layer thickness on the surface wall jet region and subsequently creating chaos in the surrounding fluid by high momentum flow [13]. Numerous research studies have been performed with a single jet and an array of jets striking on an application-oriented designed target surface. Terekhov et al. [14] and Chang and Liou [15] experimentally investigated the flow and heat transfer characteristics of jet impingement on the surface having a spherical cavity and concave/convex dimples, respectively. The local heat transfer reported for the case with a cavity on the surface was found to be lower than the flat plate/convex dimple due to the formation of vortex in the cavity. The created vortex resulted in recirculation of the heated up fluid, driving it back towards the cavity that retards the requisite heat exchange. The effusion holes were created to manage spent fluid before mixing with the fresh fluid to overcome recirculation [15-17]. Reported literature studies revealed that strength of the impinging jet and obtained hydrothermal characteristics are significantly influenced by various parameters like jet Reynolds number, jet-to-plate separation distance, physical geometry of nozzle, jet orientation, jet-to-jet distance, impinging fluid properties, target surface substrate material and geometric design [12, 18].

Interaction between neighbouring jets and jet fluid cross-flow is an intricate process that significantly influences the intensity of heat transfer and the uniformity of thermal load on the target surface. Lee et al. [19] performed an experimental analysis to evaluate the difference in heat dissipation due to varying nozzle diameter. As the nozzle diameter increased, the potential core length increases; thus, the local Nusselt number augmented at the stagnation point indicates the amplification of jet momentum and turbulence intensity. Several research studies were conducted to determine the influence of nozzle inclination angle on the cooling characteristic of the impinging jet. Heo et al. [20] optimised the heat transfer performance of single elliptic nozzle jet impingement with cross-flow in terms of Nusselt number for two design variables such as aspect ratio and inclination angle and found that inclination angle causes more influence on the elliptic jet nozzle performance than aspect ratio. Ingole and Sundaram [21] investigated heat transfer characteristic for 15° to 75° inclined jet nozzle impingement on target plate and obtained the least average Nusselt number for 15° inclined nozzles due to the detachment of flow from the target surface while 45° and 60° inclinations showed better cooling performance. Choo et al. [22] experimentally determined the effect of inclined slot jet on heat transfer performance. Parameters were compared for inclination angle varied from 0° to 40° and for a jet to plate distance less than or greater than the nozzle diameter. For the fixed flow rate condition, at a small separation distance between nozzle and target plate, the average Nusselt number increased with the elevation in inclination angle, but it decreased for large separation distance due to momentum loss. While for fixed pumping power condition, average Nusselt number noticed consistent with increased inclination angle at both small and large separation distance.

Hybrid heat sink design employs two or more cooling strategies together in a common heat sink structure such as jet impingement, microchannel flows, secondary flows, flow obstructions, nanofluids etc., to enhance heat transfer or to improve performance at low cost. Tran et al. [23] reported that reducing the channel length of multi-nozzle microchannel heat sink from 10 mm to 1 mm can aid to achieve more uniform temperature distribution and reduced thermal resistance. Moreover, pressure drop was also decreased by almost 12 times and thus improved the thermodynamic performance index. The optimum case of this novel design could handle heat flux up to 1300 W/cm^2 while keeping the temperature rise below 77.5 °C. Miry et al. [24] proposed a microchannel heat sink with an elliptical cross-section where Al_2O_3-water nanofluid jet was impinged tangentially and found that thermal resistance was reduced more than 15 % and consecutively heat transfer raised by 16 %. Naphon et al. [25] conducted an experiment for the hydrothermal performance of a heat sink impinged with a jet of TiO_2 nanofluid. They found a significant influence of nanoparticle concentration on convective heat transfer. Results revealed that convection heat transfer coefficient rises and pressure drop falls with increasing nozzle diameter and decreasing jet to plate distance. Lo and Liu [26] carried out an experimental study for thermal characteristics of multiple jet impingement over half-rough, half smooth surface where rough surface consisted of parallel or transverse grooves aligned with the jet. It was observed that the cooling performance of the half rough surface is better than the fully rough surface. However, heat transfer was more near the groove edge, and it diminished inside the grooves. Considering three different orientation of exit flow that is parallel, reverse and both side-flows showed that different cross-flow patterns have a significant role in enhancing heat transfer and flow exiting from both sides proved better than other cross-flow patterns.

Wu et al. [27] proposed a characteristic comparison of a micro-nozzle jet impingement hybrid body cooling device with a traditional surface cooling device. It was shown that the body cooling method performed more efficiently than only surface cooling technique as it provides cooling of top surface as well as side surfaces. Sung and Mudawar [28] presented a report on the hydrothermal performance of a hybrid heat sink with a row of jet impinging in a microchannel where nozzle diameter was varied in three different patterns, i.e., increasing, decreasing and equal size jet. The highest heat transfer coefficient and the lowest wall temperature were obtained for a decreasing jet diameter pattern, but the wall temperature was distributed more uniformly for equal size jet nozzle. However, when the jet size increased, spent fluid was restricted at the outlet yielding a complex flow pattern and the highest wall temperature. Husain and group did several studies considering a combination of jet impingement with microchannel heat sink [29] comprising of effusion holes [16, 17] to treat spent fluid or pillar to obstruct the fluid flow along the microchannel path [30].

Limited research studies have explored the effect of varying

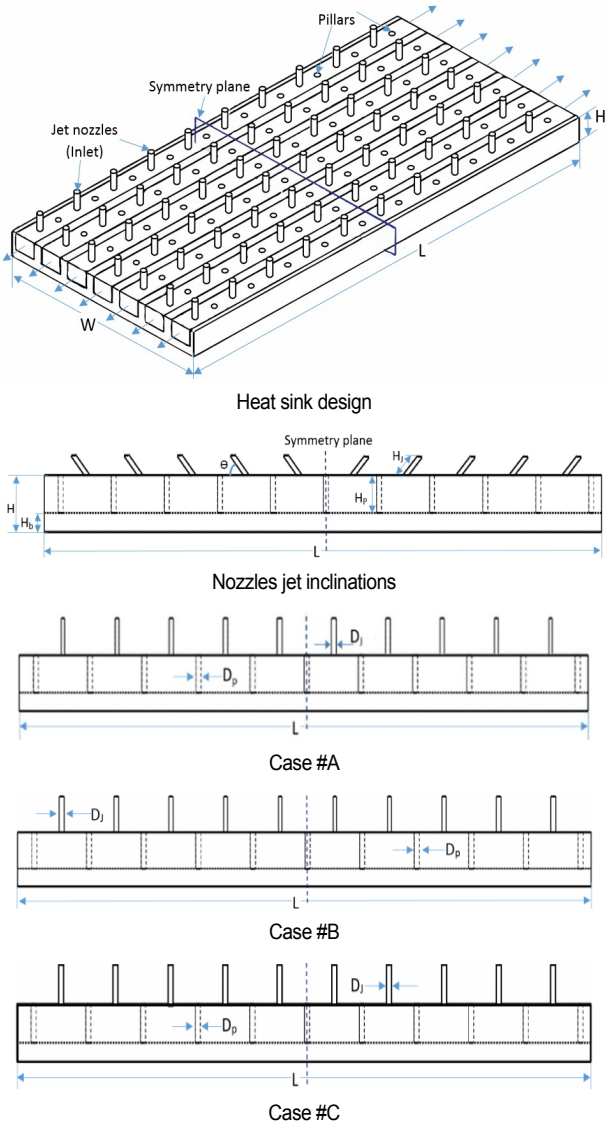

Fig. 1. Schematic of micro-jet impingement microchannel heat sink design and its proposed nozzle geometric modifications. The diameters are gradually decreased in case #A, increased in case #B and kept constant in #C along the channel length.

nozzle geometry on the performance of hybrid microchannel heat sink comprising of impinging jet and obstacle in the flow domain similar to the study reported by Husain et al. [30]. Comparative study is done for nozzle jet impinging angle varied from 30°-90° as well as for jet nozzle diameter increased/decreased along the downstream. To analyse its influence on the micro-jet impingement microchannel heat sink (MJI-MCHS) hydrothermal performance, characteristic parameters related to flow dynamics, first law of thermodynamics and second law of thermodynamics are observed.

2. Numerical modeling and analysis

Fig. 1 shows the schematic of the 24×21 mm^2 hybrid micro-

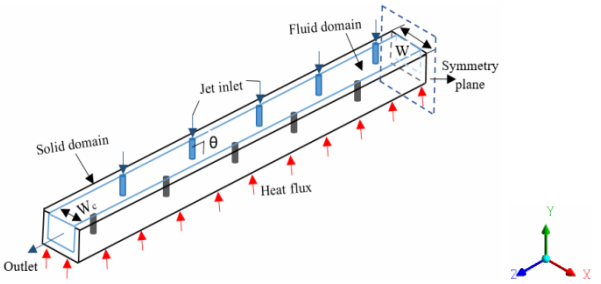

Fig. 2. Computational domain of MJI-MCHS.

channel heat sink design comprising of jet impingement and micro-pillars in the flow path. It consists of parallel microchannel rows containing inline and equally-spaced pillars in the middle of the channel flow domain and an equally-spaced nozzle located in between the pillars at the top cover over the heat sink. The jet of fluid strikes vertically on the heat sink bottom surface and gets deflected towards the channel outlets. Jet impingement is characterised by the high momentum impact of fluid on the target surface resulted in the thinning of the boundary layer and generation of chaos in the flow, while the inclusion of pillars bifurcates the fluid flow and enhances flow mixing. The collective effect of the characteristics of jet impingement technique and passive enhancement technique in the form of pillars resulted in enhanced heat transfer coefficient.

A 0.7×0.6 mm^2 copper single microchannel model was designed for the numerical analysis and the symmetric computational domain, as shown in Fig. 2. Channel width, channel height, substrate thickness and cover plate thickness were taken as 500 μm, 400 μm, 200 μm and 400 μm, respectively. Jet nozzle base diameter (D_J) and height (H_J) was considered equal to micro-pillar diameter (D_p) and height (H_P), i.e., 200 μm and 400 μm, respectively. Distance between the two pillars was kept 2.4 mm and a nozzle was drilled in between the two pillars (at 1.2 mm). The analysis is done to understand the role of different nozzle inclination angles (θ) 30°, 45°, 60° and 90° opposite to the fluid flow on the heat sink performance.

In addition, the effect of gradually increasing and decreasing the nozzle jet diameter towards the channel outlet is also studied. In the case of #A, the diameter was decreased gradually in four increments of 30 μm each towards the channel outlet from its base value of 200 μm. In the case of #B, the reverse is happening, and the jet diameter was increased gradually in four increments of 30 μm each towards the channel outlet to its base value of 200 μm. In other words, the jet diameter at the channel outlet is 80 μm in #A and 200 μm in #B. For a comparison, case #C is also studied wherein all the jet diameters were maintained at their base values of 200 μm.

DI water was taken as coolant, and all the modified designs were compared at Reynolds number ($Re = \rho V_{in} D_J / \mu$) in the range 200-600. DI water was injected at constant flow rate and temperature through multiple jets normal to the heated surface and was directed to flow along the channel length towards both the outlet directions. The outlets were maintained at the at-

Table 1. Thermo-physical properties of the fluid and solid substrate.

Property	DI water	Copper
Thermal conductivity, k (W/m^{2}K)	0.6	387.6
Specific heat capacity, C_p (J/kgK)	4182	381
Density, ρ (kg/m^3)	998.2	8978
Viscosity, μ (kg/ms)	0.001	-

mospheric conditions. The fluid and solid substrate properties are listed in Table 1.

Finite volume analysis software Ansys FLUENT was used to simulate a full three dimensional physical model of the hybrid microchannel heat sink. A pressure-based solver (SIMPLE) was implemented to compute the flow and heat transfer characteristic variables. Residuals assumed in the governing equations were reduced by 10^{-4} for continuity and momentum and 10^{-6} for energy to assume converged solutions. The fundamental equations entailed to compute the characteristic hydrothermal parameters to analyse the flow behaviour and temperature distribution within the heat sink are continuity, Navier-Stokes, and energy. Equations are defined for both solid and fluid domain as well as simplified for the steady, incompressible and laminar flow condition. Furthermore, the heat generation due to viscous dissipation, radiation heat transfer, and gravity effects are neglected in this study.

Fluid domain:

Continuity equation,

$$\nabla.\left(\rho V\right)=0\,. \tag{1}$$

Momentum equation,

$$V.\nabla\left(\rho V\right)=-\nabla p+\nabla.\left(\mu\nabla V\right)\,. \tag{2}$$

Energy equation,

$$V.\nabla\left(\rho CT\right)=\nabla.\left(k\nabla T\right)\,. \tag{3}$$

Solid domain:

Energy equation,

$$0=\nabla.\left(k_s\nabla T_s\right)\,. \tag{4}$$

In the numerical analysis, a constant heat flux (q'') of 100 W/cm^2 was supplied from the bottom surface of the MCHS and no-slip flow condition was assumed at all the channel walls. Fluid and solid properties were considered temperature independent, and thermal contact resistance was neglected. The remaining walls except the bottom were supposed to be adiabatic, which means heat loss to the ambient was neglected. Boundary conditions imposed on the computational fluid domain is illustrated in Fig. 2 and explained below in mathematical terms.

Jet inlet: $u = 0$, $v = V_{in}$, $w = 0$, $T = T_{in} = 300$ K.

Channel outlet: $P = P_{out}$ and $\dfrac{\partial T_f}{\partial n}=0$.

The interface between fluid and solid:

$u = v = w = 0$, $-k_s\dfrac{\partial T_s}{\partial n}=-k_f\dfrac{\partial T_f}{\partial n}$, $T_s = T_f$.

Wall of the domain:

At bottom surface:

$-k_s\dfrac{\partial T_s}{\partial X}=q''$ = 100 W/cm^2, u = v = w = 0 (no slip).

Other walls and symmetrical interfaces:

$\dfrac{\partial T_S}{\partial n}=0$ (adiabatic), u = v = w = 0 (no slip).

The heat sink performance was also evaluated and discussed from both the first and the second laws of thermodynamics from the hydrodynamic point of view. Characteristic parameters such as maximum wall temperature at the bottom surface ($T_{w,max}$), pressure-drop (ΔP), average heat transfer coefficient (h_{avg}), maximum thermal resistance (R_{th}), pumping power (P_P), thermal entropy generation rate (S_{gh}), and frictional entropy generation rate (S_{gf}) were observed. Thermal resistance acts as an obstruction in achieving the cooling objective which is defined as the ratio of the maximum temperature rise ($\Delta T_{\max}=T_{w,\max}-T_{in}$) and the total heat supplied, given as:

$$R_{th}=\Delta T_{w,\max}/q''A_W \tag{5}$$

where T_{in} is the fluid inlet temperature and A_w is wall surface area. Similarly, the average heat transfer coefficient determines the amount of convection heat transfer taking place within the system and it is expressed as:

$$h_{avg}=q''/\left(T_{w,avg}-T_{in}\right) \tag{6}$$

where, $T_{w,avg}$ is the average temperature at the bottom surface of the channel, and T_{in} is the inlet temperature of the fluid. Pumping power is the external energy required to provide the required volumetric flow rate $(\dot{v})$ to the fluid and is defined as $P_P=\dot{v}\Delta P$, where, ΔP *is* pressure drop across the channel.

The entropy generation rate defines the increase in the entropy of the system in an irreversible process. In the heat sink system, exchange of heat and exchange of momentum both are responsible for augmenting the entropy, collectively called the total entropy generation, S_t. Local thermal entropy generation, S'_{gh} and local frictional entropy generation, S'_{gf} expressed mathematically as [31, 32];

$$S'_{gh}=\frac{k}{T^2}\left[\left(\frac{\partial T}{\partial x}\right)^2+\left(\frac{\partial T}{\partial y}\right)^2+\left(\frac{\partial T}{\partial z}\right)^2\right], \tag{7}$$

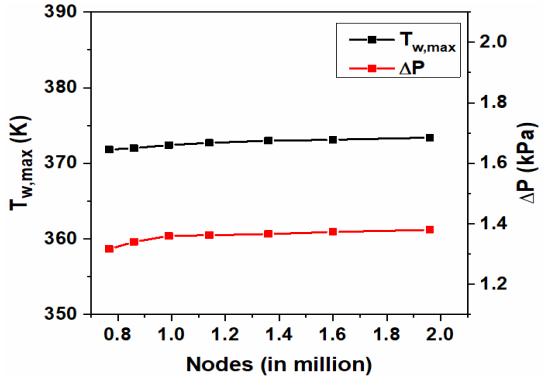

Fig. 3. Grid independency test.

$$S'_{gf} = \frac{\mu}{T}\left\{2\left[\left(\frac{\partial u}{\partial x}\right)^2+\left(\frac{\partial v}{\partial y}\right)^2+\left(\frac{\partial w}{\partial z}\right)^2\right]+\left(\frac{\partial u}{\partial y}+\frac{\partial v}{\partial x}\right)^2+\left(\frac{\partial u}{\partial z}+\frac{\partial w}{\partial x}\right)^2+\left(\frac{\partial v}{\partial z}+\frac{\partial w}{\partial y}\right)^2\right\}, \quad (8)$$

$$S'_t = S'_{gh} + S'_{gf} . \quad (9)$$

And, global entropy generation is calculated by integrating the local terms in the whole volume

$$S_{gh} = \int S'_{gh} d\forall \ , \ S_{gf} = \int S'_{gf} d\forall \ , \ S_t = \int S'_t d\forall \ .$$

A mesh independence test was conducted, shown in Fig. 3, to substantiate that the characteristic parameters remain invariant with the change in the grid size within a specific range. Accordingly, element size was varied to get nodes between 0.7 million and 2.0 million. Negligible difference between the characteristic variables such as pressure drop and maximum temperature was obtained for the node values between 1.2-1.4 million. The final grid size was considered in such a way that the most accurate results can be obtained within a short computation time.

3. Results and discussion

Validation studies were performed to ascertain the appropriateness of the numerical models and the solution procedure adopted in this study. Fig. 4 shows the comparison between the present numerical analysis results and experimental works of Tuckerman and Pease [1] for fluid flow in a microchannel and Wang et al. [33] for jet-impingement. A 50 μm wide and 300 μm deep single microchannel [1] was selected for laminar flow in parallel channels validation. The heat flux and boundary conditions were kept the same as provided in the references. Further, validation of the current numerical model was carried out by reproducing the experimental results of Wang et al. [33]. A design with 9 staggered jets of 50 μm diameter was selected for validation under the same operating conditions at a flow

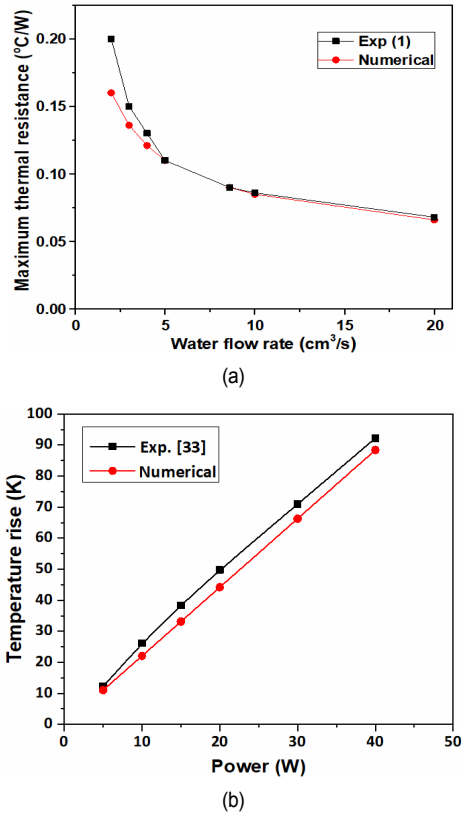

Fig. 4. The numerical and experimental results are compared to validate the numerical model for (a) microchannel heat sink; (b) jet impingement techniques.

rate of 8 ml/min [33] with experimental results. Results obtained through numerical simulation are in reasonable agreement with the experimental results and therefore attest to the veracity of the numerical procedure adopted here. The slight difference in experimental and numerical results can be attributed to the ideal symmetric and adiabatic conditions applied in the reduced numerical model; however, the experiments were performed for the full-scale model with realistic experimental conditions, which introduced some uncertainties in the results.

High flow rate resulting from high Reynolds number helped impinging jet impact at the bottom surface with more energy and thus enhanced the local turbulence in the flowing fluid and reduced wall temperature. It can be observed from the velocity and temperature distribution as shown in Fig. 5 at the mid-plane along the axial channel length. An increase in *Re* from 200 to 600 reduced the $T_{w,max}$ by about 5.5 % for 30° nozzle and 7 % for 90° nozzle. The effect of jet nozzle angles on the maximum wall temperature and pressure drop is shown in Fig. 6. Lower wall temperature indicates better substrate cooling and heat sink performance. Wall temperatures were found to reduce at high *Re* values as well as at lower jet angles. It indicates that with decreasing the nozzle angle from 90°, sweeping effects are generated and become dominant at higher *Re*. It significantly reduced the boundary layer thickness and therefore improved the mixing between the fluid layers. Contrary to

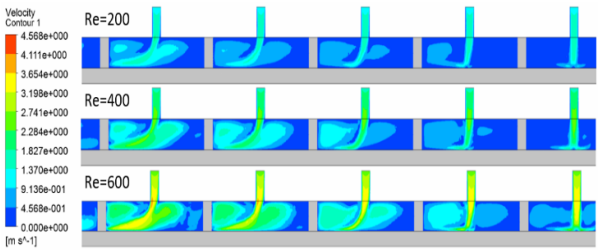

(a) Velocity distribution

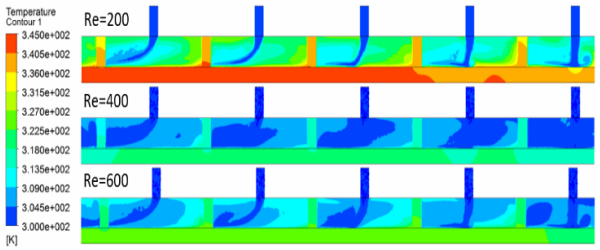

(b) Temperature distribution

Fig. 5. Velocity and temperature contours in y-z plane for different Reynolds number.

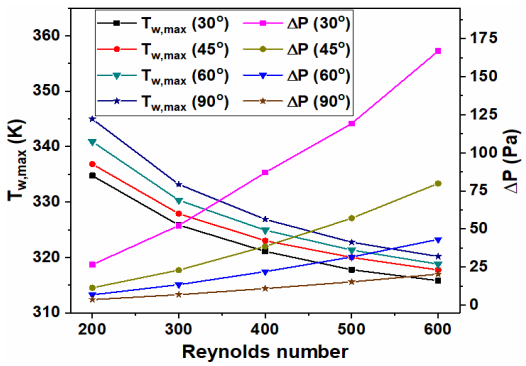

Fig. 6. Variation of maximum wall temperature and pressure drop with *Re* for different nozzle inclination angles.

$T_{w,max}$ behaviour, pressure drop increased with increase in *Re* decrease in jet angles. Larger flow disturbances for nozzle angle less than 90° caused relatively higher pressure drops due to backflow imposed by the fluid jets injected against the main channel flow.

Figs. 7 and 8 show velocity and temperature contours within the jet impingement MCHS for different nozzle angles along the y-z (mid-plane along the length) and x-y (at z = 7.8 mm normal to the channel length) planes, respectively. It can be seen in the figure that vortices are formed near the jet stagnation point and create local mixing in the overall laminar flow in all the cases; however, mixing intensity varies with the change in nozzle angles. The nozzle was inclined such that the jet is penetrating against the channel flow, as a result, a backward flow velocity is enforced in the unidirectional channel flow. Additionally, in the case of the smaller nozzle angle, the jet travelled a longer path against the bulk flow and disturbed larger

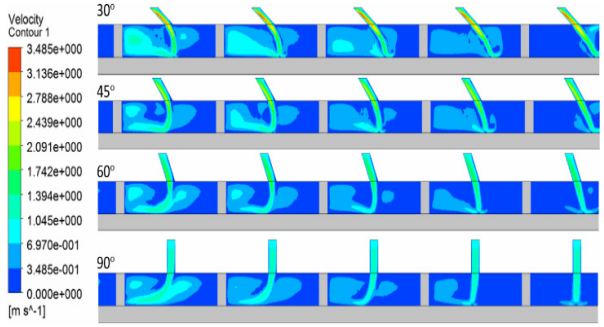

(a) Velocity distribution

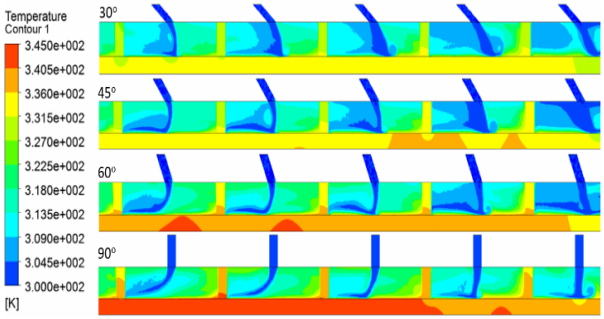

(b) Temperature distribution

Fig. 7. Velocity and temperature contours in y-z plane for different nozzle inclinations.

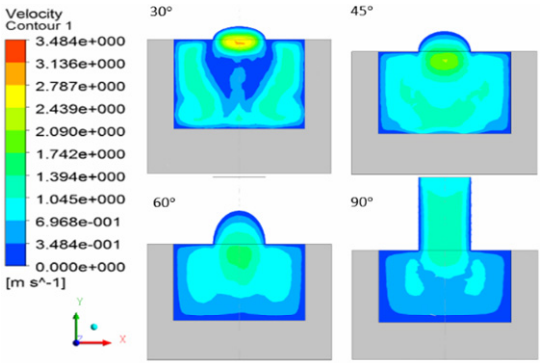

(a) Velocity distribution

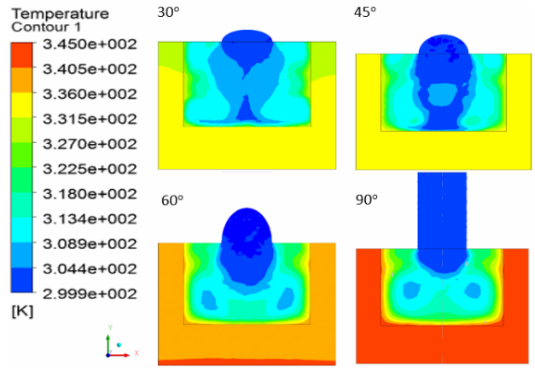

(b) Temperature distribution

Fig. 8. Velocity and temperature contours in x-y plane (normal to the channel length) for different nozzle inclinations at z = 7.8 mm.

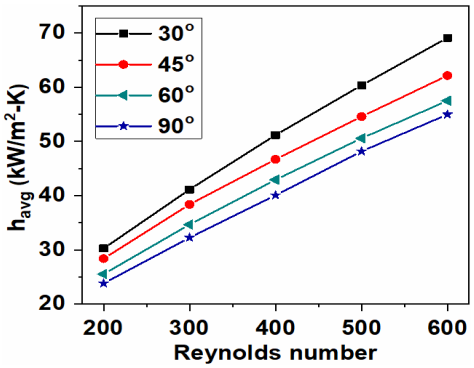

Fig. 9. Variation in average heat transfer coefficient with *Re* for different nozzle inclinations.

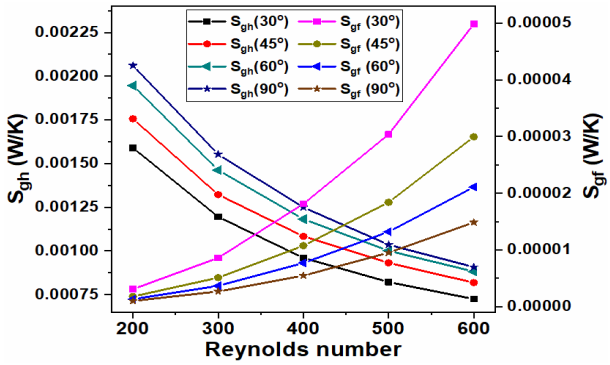

Fig. 11. Variation in thermal and frictional entropies generated for different nozzle inclinations.

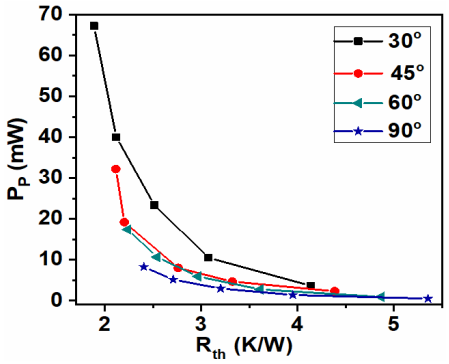

Fig. 10. Variation in P_P with the R_{th} for different nozzle inclinations.

fluid volume before striking at the base of the channel.

Therefore, as the nozzle angle decreased, more back flow was imposed on the fluid due to higher intrusion path that caused more chaos in the bulk flow. Hence, higher intensity vortices were produced, resulting in an increase in recirculation in the sweeping flow with a decrease in jet angle. This results in lowering bottom surface temperatures as well as elevating temperature uniformity at the bottom surface. Based on the result shown in Figs. 5-8, it can be concluded that 30° is the most suitable nozzle angle for enhancing the heat sink cooling performance.

The average heat transfer coefficient variation with the Reynolds number for different nozzle angles is shown in Fig. 9. Increasing Re from 200 to 600 nearly doubled the h_{avg} values, with the most improvement seen in 30° case. This can be attributed to the increase in the convection heat transfer with the increase in the flow velocity. For a given *Re*, the h_{avg} increased by 25-27 %, decreasing the nozzle angle from 90° to 30°. As a longer intrusion path was available in the case of the 30° nozzle angle, the higher mixing was observed as a consequence of the enhancement in local turbulence with a thin boundary layer and better fluid mixing. All these factors induce chaotic advection and thus facilitate escalating the convection heat transfer coefficient.

Fig. 10 shows the thermal resistance with respect to pumping power required. Thermal resistance describes the quantity of resistance present within a system during the heat exchange process. As the flow rate was increased, the thermal boundary layer in the sweeping flow was reduced that assisted in lowering the corresponding R_{th}. However, higher R_{th} was noted for smaller jet angles under the constant pumping power. This happened because of the chaos induced in the larger volume of the fluid by the small nozzle angle that resulted in higher ΔP with respect to the larger nozzle angle for the same flow rate. As pumping power is directly related to the ΔP and flow rate, a higher P_p was required to induce equivalent R_{th} for the low nozzle angle at the same flow rate.

Fig. 11 presents the variation of thermal and frictional entropy generation rates with the Reynolds number for different nozzle angles. According to the second law of thermodynamics, entropy generation rate determines work output loss due to irreversibility within the system. It was observed that the S_{gh} diminishes by almost 54-56 % in all the cases, with increasing the *Re* from 200 to 600. It means that at larger *Re*, available work-loss was less owing to higher utilisation of the fluid for the cooling purpose. Fig. 11 also shows friction entropy generation rate, which defines the loss of work because of the friction between fluid layers as well as the resistance offered on the fluid by the solid surface. Irrespective of the nozzle angle, an increase in the S_{gf} was found with increasing *Re*. As fluid velocity is higher at high *Re* and friction loss is a direct function of the flow velocity. Therefore, there would be more frictional losses at higher *Re*. This is also validated through thermodynamics second law that there are higher frictional losses at high *Re*. At a fixed *Re*, higher S_{gf} was obtained at 30° nozzle angle that further decreases as the nozzle angle increased. That is with varying the nozzle angle from 30° to 90°, invariant of the *Re*, S_{gf} was diminished by approximately 3 times. As the contact between the fluid jet and the surrounding fluid increases with decreasing the nozzle angle, higher resistance was offered. This has induced more irreversibility within the heat sink system and hence S_{gf} was escalated.

Fig. 12 shows the effects of the nozzle jet diameter layouts on the maximum wall temperature and pressure drop for different *Re* values. Reynolds number was calculated with the base

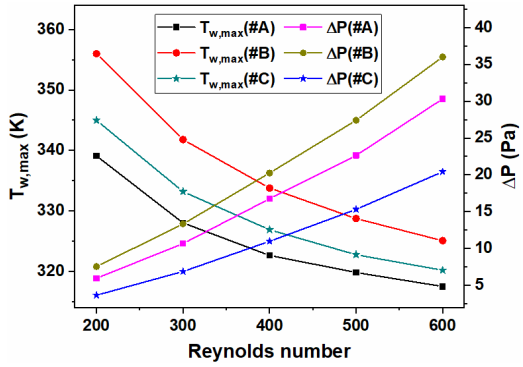

Fig. 12. Variation of maximum wall temperature and pressure drop with Re for different jet diameter sequences.

value of jet diameter (D_J = 200 μm) at a constant mass flow rate for all layouts. The #A shows the best temperature results, whereas #C shows the best results for pressure drop. In other words, using equal jet diameters is the best design for achieving low pressure drops. To better explain this behaviour, contour plots of velocity and temperature are presented next.

Figs. 13 and 14 show the velocity and temperature distribution contours for different jet diameter patterns in y-z (mid-plane) and x-y plane (at z = 7.8 mm for velocity, and z = 7.8 mm for temperature), respectively. Velocity contours demonstrate that vortices form near the stagnation point and its size and intensity grow at the next stagnation point downstream towards the outlet. The #A showed larger vortices, and #B showed the smallest size vortices. Vortices formation within the channel indicates recirculation and transverse flow due to the induction of local turbulence. The larger diameter jets impinged in the upstream region carried away a significant amount of heat from the heated surface with a larger area of wall jet as exhibited in #A and was followed by #C. The flow rate was increased due to downstream impingements as the fluid moved towards the outlet. The downstream movement of flow was accompanied by higher bulk flow mixing, resulting in a continuous decrease in surface temperature in the flow direction, as evident in Fig. 13. However, a higher pressure drop was exhibited in #A as compared to #C due to higher pressure drop exerted by small diameter jets.

The smaller diameter jets lead to shorter wall jet region and low flow rate which results in a significantly low rate of heat removal in the upstream region in #B. As a result, a higher surface temperature was observed near the upstream region. The impingements with higher jet diameter increased wall jet region and channel bulk flow as the flow moved downstream. As a result, thermal resistance was reduced, which lead to a decrease in surface temperature. The larger diameter downstream jets created a significant blockage in the bulk channel flow that resulted in a significant increase in pressure drop in #B.

The most uniform surface temperature was observed in case A and while case C exhibited the least uniform surface temperature. Lower surface temperatures were observed towards

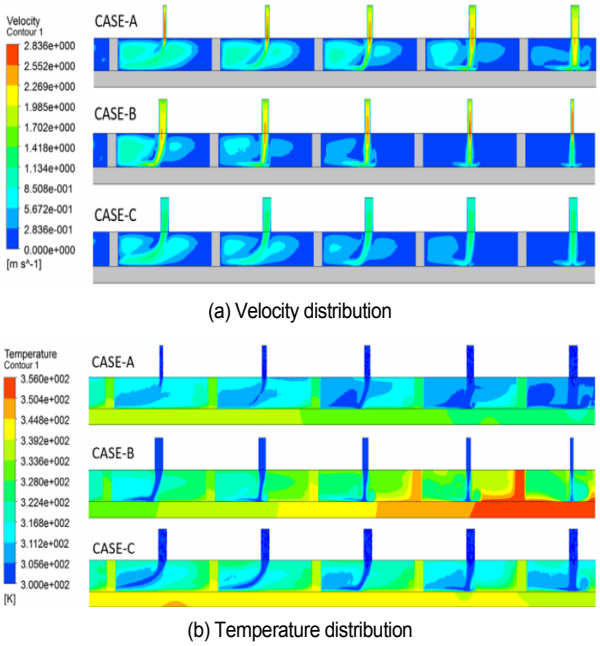

(a) Velocity distribution

(b) Temperature distribution

Fig. 13. Velocity and temperature contours in y-z plane for different jet diameter sequences.

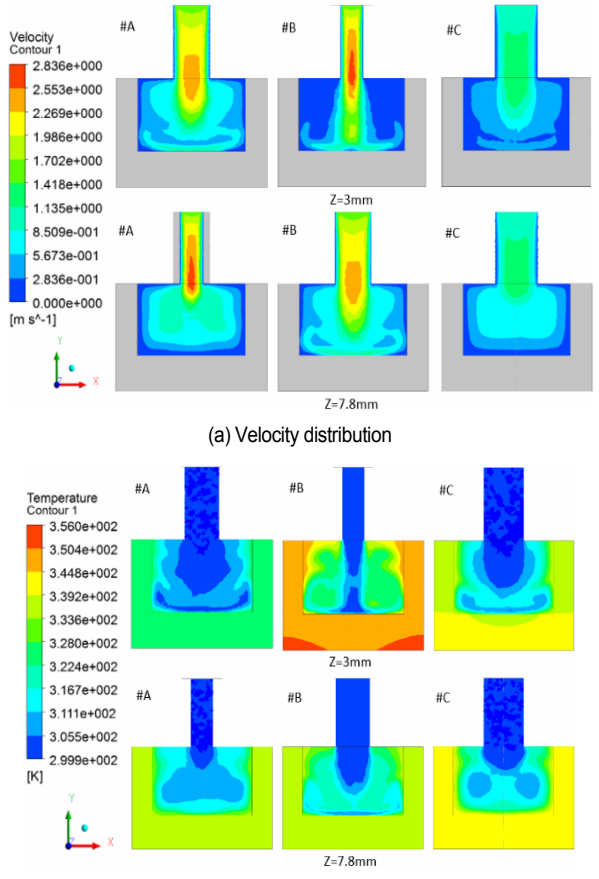

(a) Velocity distribution

(b) Temperature distribution

Fig. 14. Velocity and temperature contours in x-y plane for different jet diameter sequences at z = 3 mm and z = 7.8 mm.

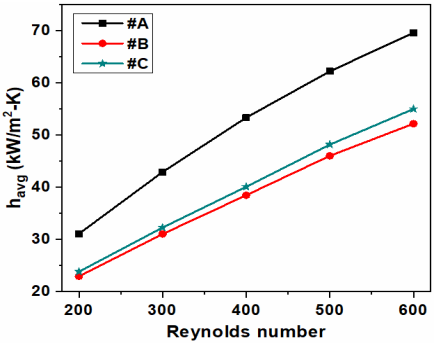

Fig. 15. Variation of h_{avg} with the *Re* for decreasing/increasing/equal nozzle diameter.

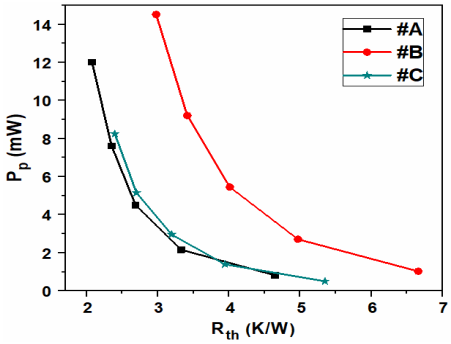

Fig. 16. Variation of P_P with R_{th} for decreasing/increasing/equal order nozzle diameters along the channel length.

the upstream in #A, and #C, which is conventional for the parallel channel flows; however, an opposite trend was observed in #B. For cases #A and #C, it occurred mainly because of the temperature difference between fluid and solid surface diminished along the length and thus the rate of heat transfer was also subdued. It can be noted in Figs. 13 and 14 that there is no definite pattern in the mixing of spent fluid with the fresh fluid in downstream that results in the rising of the average fluid temperature. Also, the impact of the impinging jet lowered towards the outlet as the boundary layer of the sweeping fluid thickens along the channel flow path that obstructed the effective heat transfer between the fluid and the solid surface. However, a reverse pattern of temperature distribution was observed in #B. The upstream flow rate was relatively smaller due to smaller diameter jets resulting in higher convective thermal resistance, which enhanced the surface temperature in the upstream zone in #B. The jet diameter increases in the downstream direction, resulting in higher flow rate, consequently reducing the convective thermal resistance. As a result, the surface temperature is reduced in the downstream zone in case B.

Fig. 15 compares the average heat transfer coefficient for the three different patterns of varying nozzle diameter at different Reynolds numbers. As the *Re* directly depends upon the flow rate, increasing the *Re* from 200-600 increased the convection heat transfer. The maximum h_{avg} was obtained in #A followed by #C and #B. At *Re* 200, #A provided an almost 30 % rise in h_{avg} while #B showed a slight reduction compared with #C. However, at *Re* 600, the h_{avg} was raised by about 26 % for #A and lowered by 5 % for #B with respect to #C. The escalation of the heat transfer in #A relative to #C was due to the larger wall jet region created by larger diameter jets at the upstream and smaller diameter jets downstream to effectively disrupt the parallel flow. Whereas, lowering of heat transfer in #B relative to #C was due to the ineffectiveness of small diameter upstream jets to lower the wall temperature as well as flow obstruction by the larger diameter downstream jets which caused thick boundary layer formation. Based on the results, it can be concluded that #A is the best layout for increasing h_{avg} as well as decreasing wall temperature.

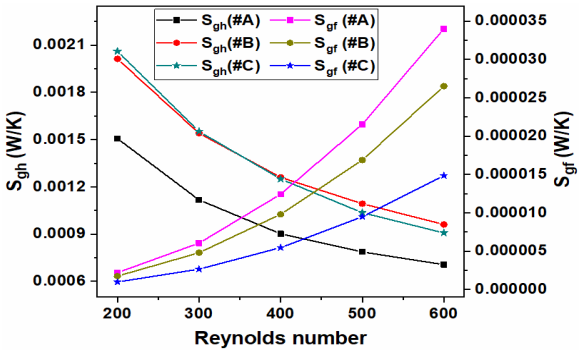

Fig. 17. Variation in thermal and frictional entropies generated for decreasing/increasing/equal nozzle diameter.

Thermal resistance offered in #A, #B and #C at various pumping powers are shown in Fig. 16. It was noticed that higher pumping power produces lower thermal resistance and vice versa because of the thinning of the boundary layer. For the same R_{th}, the highest P_P was used by the #B due to the highest obstructions in fluid flow caused by the jets in the form of large stagnation zones, see Fig. 13. Therefore, in order to decrease the equivalent R_{th}, P_P demand increased in #B than in other cases. However, P_P required in #A case is slightly less than the #C case owing to higher flow velocity for the same volume flow rate. Thus, we can conclude that increasing nozzle diameter towards flow can cost remarkably more while decreasing diameter can cut cost with respect to equal diameter case to maintain the equivalent thermal resistance within the heat sink.

Fig. 17 presents the variation of thermal and frictional entropy generation at different Reynolds number. It can be seen that S_{gh} decrease by about two times with the increase of *Re* in all the cases. It is because of the occurrence of greater heat transfer and smaller work losses at higher *Re* that further diminish the system's irreversibility, thus resulting in lowering system entropy. Minimum S_{gh} was obtained for the #A while #B and #C showed an almost equivalent value of the S_{gh}. At *Re* 200, S_{gh} for #A was almost 27 % lower than #C, while at *Re* 600, it was nearly 22 % lower. This is validated through second law analy-

sis that minimum heat exchange losses occur in the #A and thus, it produced lower irreversibility within the system.

Friction entropy generation results show a significant increase in S_{gf} with Re. The minimum value of the S_{gf} was found in #C, while the maximum value was in #A. It simply means that system irreversibility has increased considerably due to the larger resistance offered against the fluid flow. Higher chaos of the fluid in #A resulted in higher frictional losses in comparison to #C. Similar to #A, higher values of the S_{gf} in #B imply that frictional losses are more due to the higher average velocity and more disturbance within the system. However, higher flow obstruction in the downstream in #B case lessened the velocity gradient along the length and thus, reduced the S_{gf} with respect to #A case.

4. Conclusions

The present study focused on the improvement of the hybrid heat sink flow and thermal characteristics using several geometric and flow variables. Jet impingement nozzle and pillars were integrated with the microchannel heat sink to utilise the synergetic effects in elevating cooling performance. Geometric variables included nozzle inclination angle varied from 30° to 90° and nozzle diameter increased/decreased equally along with the channel flow while flow variable included Reynolds number varied from 200 to 600. Pressure drop and pumping power were evaluated to analyse the hydraulic performance, and thermal and frictional entropy generation rate were computed to investigate thermal performance on the second law of thermodynamics basis. Likewise, thermal resistance, maximum wall temperature and average heat transfer coefficient were evaluated to explore the thermal performance on the first law of thermodynamics basis. It was observed that $T_{w,max}$ increases with increasing the nozzle angle from 30° to 90°. Similarly, S_{gh} was augmented by 25-30 % with an increase in the nozzle impingement angle from 30° to 90°. However, an extreme rise in the ΔP and S_{gf} was seen with decreasing the nozzle angle. Due to the longer jet travel path available at a lower angle, higher chaotic advection occurred that increased the heat transfer as well as frictional losses within the heat sink. Decreasing nozzle diameter (#A) along the channel length provided the lowest $T_{w,max}$ and S_{gh} among all other varying diameter patterns considered. Moreover, higher heat transfer coefficient and more uniform temperature distribution were obtained for #A. On the other hand, ΔP and S_{gf} showed significant elevation in #B and #A with respect to the #C case. For every geometric variation, $T_{w,max}$ decreases and h_{avg} increases with increasing the Re. However, increasing Re also resulted in a pressure drop hike for all the geometric variations. While considering all the cases in the present study, it can be concluded that an improvement in thermal performance is always associated with the rise in pressure drop. Therefore, it is necessary to optimise the geometric design of the jet impingement microchannel heat sink based on the relative significance of the performance parameters.

Acknowledgments

This work was supported by IIITDM Jabalpur, India.

Nomenclature

A_w : Wall surface area (m^2)
C : Specific heat capacity (J/kg-K)
D : Diameter (m)
D_h : Hydraulic diameter (m)
H : Height (m)
h : Heat transfer coefficient (W/m^2-K)
k : Thermal conductivity (W/m-K)
L : Length (m)
n : Normal direction (m)
Nu : Nusselt number
ΔP : Pressure drop across MCHS (Pa)
P : Pressure (Pa)
P_P : Pumping power (W)
q'' : Heat flux (W/cm^2)
R_{th} : Thermal resistance (K/W)
Re : Reynolds number
S : Entropy generation (W/K)
T : Temperature (K)
u : Velocity in x-direction (m/s)
V : Velocity (m/s)
$\forall$: Volume (m^3)
$\dot{v}$: Volumetric flow rate (m^3/s)
v : Velocity in y-direction (m/s)
W : Width (m)
w : Velocity in z-direction (m/s)
x : X-coordinate (m)
y : Y-coordinate (m)
z : Z-coordinate (m)

Greek symbols

μ : Viscosity (kg/m-s)
ρ : Density (kg/m^3)
θ : Nozzle inclination angle

Subscripts

avg : Average
b : Base
c : Channel
f : Fluid
gh : Thermal
gf : Frictional
in : Inlet
J : Nozzle jet
max : Maximum
out : Outlet
p : Pillar
s : Solid

t : Total
w : Wall

References

[1] D. B. Tuckerman and R. F. W. Pease, High-performance heat sinking for VLSI, *IEEE Electron Device Lett.*, EDL-2 (5) (1981) 126-129.

[2] J. Pandey, M. Z. Ansari, A. Husain and M. A. Ansari, Comparative study of flow characteristics in uniformly varying microchannel for di water and nanofluid, *AIP Conf. Proc.*, 2105 (1) (2019) 020016.

[3] J. Pandey, M. Z. Ansari and A. Husain, Numerical simulation of heat transfer in gradually varying microchannel heat sink, *IOP Conf. Ser. Mater. Sci. Eng.*, 691 (1) (2019) 012069.

[4] N. A. C. Sidik, M. N. A. W. Muhamad, W. M. A. A. Japar and Z. A. Rasid, An overview of passive techniques for heat transfer augmentation in microchannel heat sink, *Int. Commun. Heat Mass Transf.*, 88 (2017) 74-83.

[5] G. Krishan, K. C. Aw and R. N. Sharma, Synthetic jet impingement heat transfer enhancement-a review, *Appl. Therm. Eng.*, 149 (2019) 1305-1323.

[6] H. H. Jasim and M. S. Söylemez, Optimization of a rectangular pin fin using elliptical perforations with different inclination angles, *J. Mech. Sci. Technol.*, 31 (10) (2017) 5029-5039.

[7] J. T. Choi, O. K. Kwon and D. A. Cha, A numerical study of the heat transfer and fluid flow of micro-channeled water block for computer CPU cooling, *J. Mech. Sci. Technol.*, 25 (10) (2011) 2657–2663.

[8] S. Xu, G. Hu, J. Qin and Y. Yang, A numerical study of fluid flow and heat transfer in different microchannel heat sinks for electronic chip cooling, *J. Mech. Sci. Technol.*, 26 (4) (2012) 1257-1263.

[9] D. Kim, C. H. Yu, S. H. Yoon and J. S. Choi, Effects of manifold geometries on flow distribution to parallel microchannels, *J. Mech. Sci. Technol.*, 25 (12) (2011) 3069-3074.

[10] A. Husain and K. Y. Kim, Electroosmotically enhanced microchannel heat sinks, *J. Mech. Sci. Technol.*, 23 (3) (2009) 814-822.

[11] J. H. Park and I. S. Park, Flow distribution of two-phase fluid through multiple microchannels, *J. Mech. Sci. Technol.*, 35 (6) (2021) 2481-2492.

[12] N. Zuckerman and N. Lior, Jet impingement heat transfer: physics, correlations, and numerical modeling, *Adv. Heat Transf.*, 39 (2006) 565-631.

[13] G. M. Carlomagno and A. Ianiro, Thermo-fluid-dynamics of submerged jets impinging at short nozzle-to-plate distance: a review, *Exp. Therm. Fluid Sci.,* 58 (2014) 15-35.

[14] V. I. Terekhov, S. V. Kalinina, Y. M. Mshvidobadze and K. A. Sharov, Impingement of an impact jet onto a spherical cavity. flow structure and heat transfer, *Int. J. Heat Mass Transf.*, 52 (11-12) (2009) 2498-2506.

[15] S. W. Chang and H. F. Liou, Heat transfer of impinging jet-array onto concave- and convex-dimpled surfaces with effusion, *Int. J. Heat Mass Transf.*, 52 (19-20) (2009) 4484-4499.

[16] A. Husain, N. A. Al-Azri, N. Z. H. Al-Rawahi and A. Samad, Comparative performance analysis of microjet impingement cooling models with different spent-flow schemes, *J. Thermophys. Heat Transf.*, 30 (2) (2016) 465-471.

[17] A. Husain and M. Ariz, Thermal performance of jet impingement with spent flow management, *Int. J. Eng. Trans. A Basics*, 30 (10) (2017) 1599-1608.

[18] M. Molana and S. Banooni, Investigation of heat transfer processes involved liquid impingement jets: a review, *Brazilian J. Chem. Eng.*, 30 (3) (2013) 413-435.

[19] D. H. Lee, J. Song and M. C. Jo, The effects of nozzle diameter on impinging jet heat transfer and fluid flow, *J. Heat Transfer*, 126 (4) (2004) 554-557.

[20] M. W. Heo, K. D. Lee and K. Y. Kim, Optimization of an inclined elliptic impinging jet with cross flow for enhancing heat transfer, *Heat Mass Transf.*, 47 (6) (2011) 731-742.

[21] S. B. Ingole and K. K. Sundaram, Experimental average Nusselt number characteristics with inclined non-confined jet impingement of air for cooling application, *Exp. Therm. Fluid Sci.*, 77 (2016) 124-131.

[22] K. Choo, T. Y. Kang and S. J. Kim, The effect of inclination on impinging jets at small nozzle-to-plate spacing, *Int. J. Heat Mass Transf.*, 55 (13-14) (2012) 3327-3334.

[23] N. Tran, Y. J. Chang, J. T. Teng, T. Dang and R. Greif, Enhancement thermodynamic performance of microchannel heat sink by using a novel multi-nozzle structure, *Int. J. Heat Mass Transf.*, 101 (2016) 656-666.

[24] S. Ziaedin Miry, S. Lohrasbi, H. Irani, M. Ashjaee and D. D. Ganji, Thermal energy absorption in a heat sink with elliptical cross section and tangential impinging inlet flow of nanofluid, *Exp. Therm. Fluid Sci.*, 89 (2017) 50-61.

[25] P. Naphon, L. Nakharintr and S. Wiriyasart, Continuous nanofluids jet impingement heat transfer and flow in a microchannel heat sink, *Int. J. Heat Mass Transf.*, 126 (2018) 924-932.

[26] Y. H. Lo and Y. H. Liu, Heat transfer of impinging jet arrays onto half-smooth, half-rough target surfaces, *Appl. Therm. Eng.*, 128 (2018) 79-91.

[27] R. Wu, T. Hong, Q. Cheng, H. Zou, Y. Fan and X. Luo, Thermal modeling and comparative analysis of jet impingement liquid cooling for high power electronics, *Int. J. Heat Mass Transf.*, 137 (2019) 42-51.

[28] M. K. Sung and I. Mudawar, Effects of jet pattern on single-phase cooling performance of hybrid micro-channel/micro-circular-jet-impingement thermal management scheme, *Int. J. Heat Mass Transf.*, 51 (19-20) (2008) 4614-4627.

[29] A. Husain, J. H. Kim and K. Y. Kim, Performance characterization of laminar flow in multiple microjet impingement heat sinks, *J. Thermophys. Heat Transf.*, 28 (1) (2014) 133-141.

[30] A. Husain, M. Ariz, N. Z. H. Al-Rawahi and M. Z. Ansari, Thermal performance analysis of a hybrid micro-channel, -pillar and -jet impingement heat sink, *Appl. Therm. Eng.*, 102 (2016) 989-1000.

[31] M. Bahiraei, A. Monavari, M. Naseri and H. Moayedi, Irre-

versibility characteristics of a modified microchannel heat sink operated with nanofluid considering different shapes of nanoparticles, *Int. J. Heat Mass Transf.*, 151 (2020) 119-359.

[32] A. A. A. A. Al-Rashed, A. Shahsavar, O. Rasooli, M. A. Moghimi, A. Karimipour and M. D. Tran, Numerical assessment into the hydrothermal and entropy generation characteristics of biological water-silver nano-fluid in a wavy walled microchannel heat sink, *Int. Commun. Heat Mass Transf.*, 104 (2019) 118-126.

[33] E. N. Wang et al., Micromachined jets for liquid impingement cooling of VLSI chips, *J. Microelectromechanical Syst.*, 13 (5) (2004) 833-842.

Jyoti Pandey is a Research Scholar in the Discipline of Mechanical Engineering at IIITDM Jabalpur. She received her B.E. degree from Jabalpur Engineering College, Jabalpur, India in 2015 and M.Tech. degree in Thermal Engineering in 2018 from the National Institute of Technology, Raipur, India. Her research interests include microcombustion, microfluidics and heat transfer.

Mohd. Zahid Ansari is an Associate Professor in the Discipline of Mechanical Engineering at IIITDM Jabalpur. He received his B.Tech. degree from the Aligarh Muslim University, India in 2001, and M.Tech. and Ph.D. degrees in 2006 and 2010 from the Department of Mechanical Engineering, Inha University, South Korea. His areas of interest include MEMS, microfluidics and heat transfer.

Afzal Husain is an Associate Professor in the Mechanical and Industrial Engineering Department at Sultan Qaboos University, Oman. He received B.E. and M.Tech. degrees in Mechanical Engineering from Aligarh Muslim University, India, and earned Ph.D. degree with a major in Thermodynamics and Fluid Mechanics at Inha University, South Korea. He worked as a full-time lecturer in the Department of Mechanical Engineering at Inha University from Mar. 2010 to Aug. 2012. His research interests are thermofluids & computational fluid dynamics (CFD), microfluidics, heat transfer and electronics cooling.